Controllable multiband terahertz notch filter based on a parallel plate waveguide with a single deep groove

Lin Chen,[1,2] Zhaoxiang Cheng,[1] Jiaming Xu,[1] Xiaofei Zang,[1] Bin Cai,[1] and Yiming Zhu[1,*]

[1]*Shanghai Key Laboratory of Modern Optical System and Engineering Research Center of Optical Instrument and System, Ministry of Education, University of Shanghai for Science and Technology, Shanghai 200093, China*

[2]*e-mail: linchen@usst.edu.cn*

**Corresponding author: ymzhu@usst.edu.cn*

Received May 22, 2014; revised June 30, 2014; accepted July 1, 2014; posted July 2, 2014 (Doc. ID 212599); published July 29, 2014

The influence of the air gap on the response of transmission for a transverse-electric mode parallel plate waveguide with a single deep groove has been experimentally studied. As the air gap is larger than the resonant wavelength of a high-order cavity mode in a single deep grooved waveguide, only the fundamental cavity mode can be excited and the single resonance (band) can be observed in a transmission spectrum. The decrease of the air gap can not only efficiently push the radiation of the fundamental cavity mode into the deep groove but also excite the high-order cavity modes, resulting in multiple resonances (multiband) in the corresponding spectrum. Based on the above observations, a tunable multiband terahertz notch filter has been proposed and the variation of the air gap has turned out to be an effective method to select band number. Experimental data and simulated results verify this band number tunability.

OCIS codes: (300.6495) Spectroscopy, terahertz; (260.5740) Resonance.
http://dx.doi.org/10.1364/OL.39.004541

The parallel-plate waveguide (PPWG) is a simple device in terahertz (THz) range that is well understood in classical waveguide theory and widely employed because of its low loss and low dispersion characteristics [1]. Because PPWG has the ability to confine radiation, it can be employed in conjunction with resonant structures, resulting in unique spectral resonant features that open up PPWGs to a myriad of sensing and filtering applications. There have been several designs that employed resonant structures embedded within PPWGs such as Bragg gratings, photonic band gap, and resonant groove(s) structures [2–10]. Recently, a single rectangular groove incorporated into a transverse-electric (TE) mode PPWG has been demonstrated as a notch filter, which can realize a very narrow linewidth result [11]. Compared with the transverse-electromagnetic (TEM) mode for PPWG applications [1], the TE mode PPWG is simple to machine, easy to couple from free space, and has low ohmic loss [11,12]. Astley *et al.* characterized the single groove TE mode waveguide resonant structure and analyzed the origin of the resonant behavior together with the dependence on geometric factors [13]. They found that each transmission spectrum for these grooved waveguides with constant width (460 μm) and plate separation (1 mm), but varying depth shows only one single notch resonance in the experiment. It is interesting to note that the grooved PPWG structures are analogous to plasmonic stub metal–insulator–metal structures in visible region [14–17], and the transmission spectrum exhibits multiple resonances for large stub length [16,17]. However, a similar aspect of the single grooved TE mode PPWG performance has not been sufficiently studied in the THz region. In this Letter, by adjusting the air gap, both single and multiple resonances in the transmission spectrum in single deep grooved TE mode PPWG structure are observed experimentally and revealed numerically. Then the physical origin of this phenomenon is analyzed. Compared with resonant features in similar structure presented [10,13], our results show some new features: first, the appearance of multiple resonances in the transmission spectrum with a small air gap is attributed to the existence of a high order cavity mode in the deep groove; second, the resonant frequency of the fundamental cavity mode (lowest frequency band) for the deep groove deviates from that for a shallow groove with a small air gap, because of the fact that the THz field energy has fully occupied the entire deep groove area. In addition, we demonstrate the design of a tunable multiband notch filter with a band number control by mechanically altering the air gap parameter.

Figure 1 illustrates the diagram of a simple design of the geometry of a deep grooved PPWG structure. We use a groove with a fixed width $w = 400$ μm based on a previous experiment [8,18], and set the depth to be $h = 1400$ μm as our default number. The cylindrical coupler structure and the process of mechanically tuning air gap

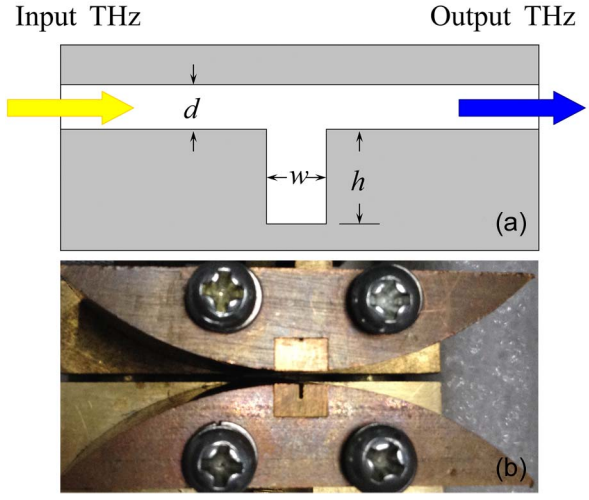

Fig. 1. (a) Structure sketch of single deep groove PPWG structure; (b) the real image of our sample. The geometry parameters of the deep groove are $w = 400$ μm and $h = 1400$ μm.

d in this Letter are identical to that of a PPWG with double grooves in our previous literature [18]. For excitation of the TE mode, the incident THz wave is applied with polarization parallel to the plates [8,18]. A photography image of the fabricated groove waveguide is shown in Fig. 1(b).

An investigation of the resonances is carried out with several experimental tests via a THz time domain spectroscopy (THz-TDS) system, as described [8,18,19]. The experimental setup has the frequency resolution of 4.58 GHz corresponding to the time domain waveforms ~218.4 ps. Figures 2(a)–2(c) show the amplitude spectra of a waveguide with (red dotted line) and without (reference, black dotted line) groove in three typical air gaps cases. Apparently, the spectra show the characteristics of single, double, and triple resonance dips for $d = 800$, 710, and 555 μm, respectively. We also obtain another amplitude spectrum from the grooved waveguide structure with air gap $d = 555$ μm as the same as Fig. 2(c), yet with different depth $h = 400$ μm, as performed in Fig. 2(d). Compared with Fig. 2(c), there is only one resonance dip in the amplitude spectrum, which agrees with the result [13]. It is worth noting that Fig. 2(a) has a resonant dip with a broader line width and lower extinction compared with results in Refs. [5,13]. These are most likely because of the lack of spectral resolution necessary to really characterize very narrow resonance, or the inevitably slight nonparallel induced by mechanically tuning the screw micrometer (see Fig. 1(a) [18]), or imperfections in the fabrication. Furthermore, the cutoff frequencies for each d and the water-vapor absorption lines (at 0.557 THz) can also been found in Figs. 2(a)–2(d) [18].

Figure 3 compares the power transmission spectra of a single deep grooved PPWG for a different air gap. Power transmission spectra were calculated by comparing the amplitude spectra of the propagated pulses with and without incorporated groove. The resonance dip at lowest frequency (marked as Band I, red arrows) is noticeable at all air gaps in each spectrum. Its frequency is changed from 0.321 to 0.38 THz when the air gap

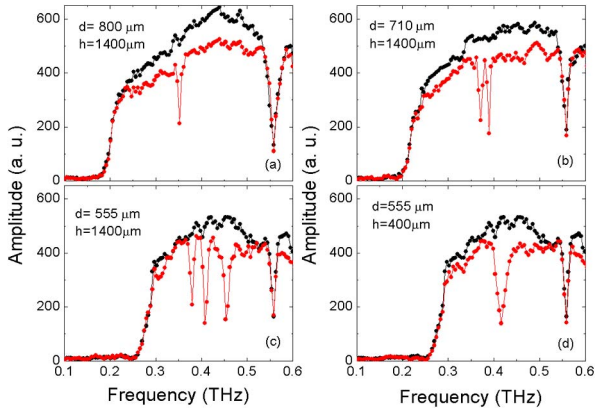

Fig. 2. Measured amplitude spectra of ungrooved (black) and grooved (red) waveguide with (a) $d = 800$ μm, $h = 1400$ μm; (b) $d = 710$ μm, $h = 1400$ μm; (c) $d = 555$ μm, $h = 1400$ μm; and (d) $d = 555$ μm, $h = 400$ μm. The dots have the frequency resolution 4.58 GHz, corresponding to 218.4 ps time-domain waveforms.

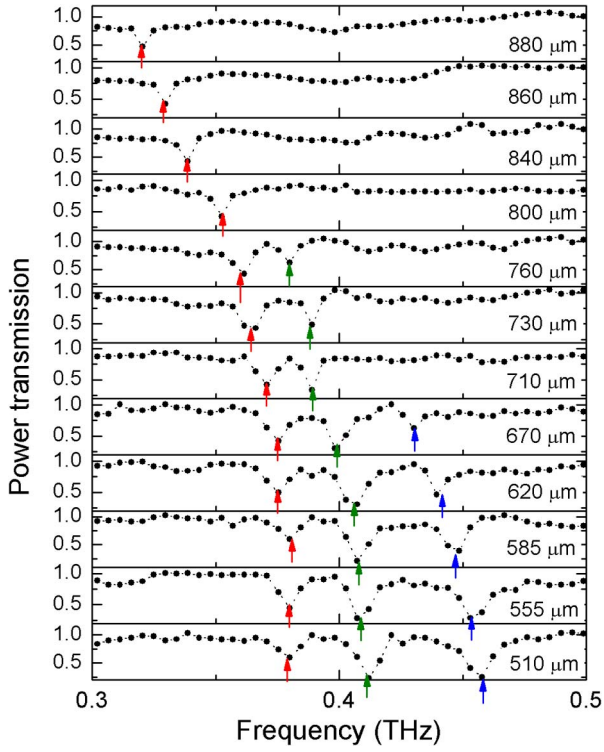

Fig. 3. Power transmission spectra for different air gap d. The spectra from d at 800, 710, and 555 μm were calculated from the data shown in Figs. 2(a)–2(c). The dots have the frequency resolution 4.58 GHz, corresponding to 218.4 ps time-domain waveforms. Arrows indicate resonance dips (red arrows, Band I; green arrows, Band II; and blue arrows, Band III).

decreases from 880 to 510 μm, respectively. Interestingly, the resonance dips of Band II (green arrows) and Band III (blue arrows) in the spectra can be seen explicitly at descending air gaps started from 760 and 670 μm, respectively. The relationship between the positions of definable dips at Band I, II, and III, and the air gap ($1/d$) is plotted in Fig. 4(a). The experimental results (dots) are well corroborated by simulated results (solid lines, COMSOL Multiphysics). We found that only Band I [Fig. 4(a), red line (dots)] exists when d is larger than 770 μm ($1/d < 1.302$ mm^{-1}). As d becomes smaller (0.302 mm$^{-1} < 1/d < 1.441$ mm^{-1}), Band II [Fig. 4(a), green line (dots)] occurs in each transmission spectrum. When d is smaller than 690 μm($1/d > 1.441$ mm^{-1}), three resonances can be found simultaneously and the highest frequency resonance contributes to the existence of Band III [Fig. 4(a), blue line (dots)]. Bands II and Band III terminate at light line (dashed line), where $1/d =$ 1.302 and 1.441 mm^{-1}, respectively. According to [18], the light line implies the condition $d = \lambda$, where λ represents a wavelength of incident THz radiation. As d increases and the resonant wavelengths of the three bands are larger than d (below the light line), triple resonances can be found obviously. Once the resonance wavelength of Band II (or III) is smaller than d, this band cannot be excited and the incident THz wave propagates along the PPWG. In addition, we plotted the trends of the Q-factor ($Q = f/\Delta f$, where f is the resonant frequency at each dip and Δf is the line width of the dip) change for three bands with the variation of the air gap, as shown in

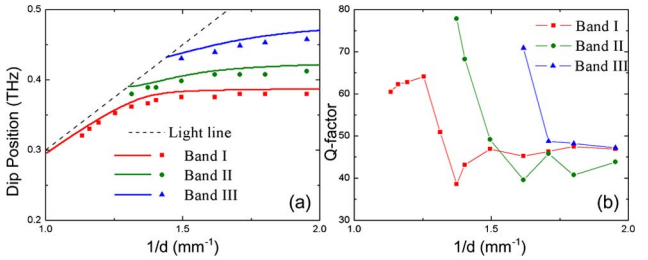

Fig. 4. (a) Positions of resonant dips of Bands I, II, and III as a function of the reciprocal of d ($1/d$). Solid lines, numerical results; dot, experimental results from power transmission spectra (Fig. 3); and dash line, the light line. Red, green, and blue colors represent Bands I, II, and III, respectively. (b) Measured Q-factor of Bands I, III, and III as a function of the reciprocal of d ($1/d$ from power transmission spectra (Fig. 3).

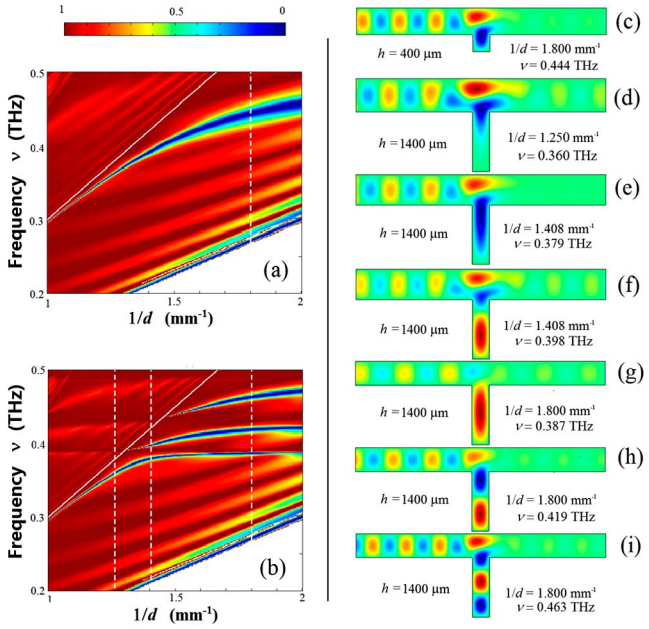

Fig. 5. (Left) Simulated transmission map as a function of $1/d$ with (a) $h = 400$ μm and (b) $h = 1400$ μm. The white solid line is the light line. The white dashed lines are the corresponding examples in the experiment [Figs. 2(a)–2(d)]. (Right) Simulated electric field distributions in the grooved waveguides with different $1/d$ [white dashed lines in (a) and (b)] at resonances. (c) $h = 400$ μm, $1/d = 1.8$ mm^{-1}, $\nu = 0.444$ THz; (d) $h = 1400$ μm, $1/d = 1.25$ mm^{-1}, $\nu = 0.36$ THz; (e) $h = 1400$ μm, $1/d = 1.408$ mm^{-1}, $\nu = 0.379$ THz; (f) $h = 1400$ μm, $1/d = 1.408$ mm^{-1}, $\nu = 0.398$ THz; (g) $h = 1400$ μm, $1/d = 1.8$ mm^{-1}, $\nu = 0.387$ THz; (h) $h = 1400$ μm, $1/d = 1.8$ mm^{-1}, $\nu = 0.419$ THz; and (i) $h = 1400$ μm, $1/d = 1.8$ mm^{-1}, $\nu = 0.463$ THz.

Fig. 4(b). The Band II at 760 μm air gap and Band III at 670 μm air gap have resonant dips with a lower extinction, which does not allow accurate determination of the line width, so these Q-factor values are excluded from the plot. Although the exact value of the Q-factor in Fig. 3 can hardly be obtained because of the resolution limit, some interesting information can be received. First, for Band I, at the beginning, the Q-factor increases a little as the air gap decreases, and corresponds to the increase in the resonant frequency. Then, the Q-factor for Bands I, II, and III experience the initial drop and then appears to be a constant with small fluctuations as the air gap decreases. The dramatic decrease for the three bands comes from the increasing loss induced by more abrupt junctions between the waveguide sections, and the following small change is because of the high energy concentration in the deep groove. The trends observed in Fig. 4(b) agree qualitatively with the simulation in Fig. 5(b). As a result, by directly changing the air gap, the band number, resonance position, and Q-factor can all be controlled.

To investigate the origin of multiple bands, we show in Fig. 5(a), $h = 400$ μm, and Fig. 5(b), $h = 1400$ μm, the two dimensional transmission maps obtained by varying the incident frequency ν and air gap ($1/d$). The white solid line is the light line and the white dashed lines stand for air gaps d of 555, 710, and 800 μm in the experiment [Figs. 2(a)–2(d)], respectively. It is found that, for $1/d < 1.302$ mm^{-1} [Band II has not been excited in Fig. 5(b)], the resonant frequency curve of Band I with $h = 1400$ μm [Fig. 5(b)] coincides with that of a single resonance band with $h = 400$ μm [Fig. 5(a)]. However, when the air gap is gradually decreased, in Fig. 5(a) there is still a single band in each transmission spectrum and the resonance shifts toward higher frequencies, while in Fig. 5(b) additional bands occur in each transmission spectrum and the resonant frequency of Band I tends to be invariable. Then we extract images of the characteristic snapshots of electric field patterns inside the waveguide at the corresponding resonances for both shallow ($h = 400$ μm) and deep ($h = 1400$ μm) grooved waveguides in Figs. 5(c)–5(i) to reveal the differences between Figs. 5(a) and 5(b). For a shallow groove ($h = 400$ μm), the image in Fig. 5(c) indicates that the cavity mode is excited at a resonant frequency of about 0.444 THz with $1/d = 1.8$ mm^{-1} ($d = 555$ μm), resulting in a transmission dip as shown in Fig. 2(d). Then we discuss the images for a deep groove ($h = 1400$ μm). First, at a resonant frequency of about 0.36 THz (Band I) with $h = 1400$ μm and $1/d = 1.25$ mm^{-1} ($d = 800$ μm), the deep groove structure exhibits its fundamental cavity mode as shown in Fig. 5(d). Meanwhile, most of the THz field occupies the air gap area and does not fully penetrate the groove, which indicates that the groove depth has little effect on the resonant frequency [10]. That is why the resonant frequency curve of Band I in Fig. 5(b) coincides with that of single resonance in Fig. 5(a) as $1/d < 1.302$ mm^{-1}. At the same time, Bands II and III cannot be seen in this case because of the fact that their resonant wavelengths are smaller than d. As air gap d is gradually decreased, for Band I, the field in the groove becomes strong [Fig. 5(e)] and the resonant frequency blue shifts. Once the top metal plate is further brought close to the bottom plate incorporated groove, the energy is fully distributed and the strength reaches very high value in the groove [Fig. 5(g)]. Here the resonant frequency of fundamental cavity mode is significantly determined by groove depth. This observation can explain the observable large deviation between the resonant frequency curve of the fundamental cavity mode in Figs. 5(a) and 5(b) with the increase in the air gap. Intriguingly, moving the top plate toward the bottom by decreasing air gap d seems to push the electromagnetic wave into the deep groove, as shown in

Figs. 5(d), 5(e), and 5(g). In addition, as d is decreased, the high order cavity modes can be excited. For example, Band II can be excited at the resonant frequency 0.398 THz for a gap of $d = 710$ μm ($1/d = 1.408$ mm^{-1}), as shown in Fig. 5(f). It also shows a little blue shift to 0.419 THz as $1/d$ is increased to 1.8 mm^{-1} [$d = 710$ μm, Fig. 5(h)]. Here, the resonant wavelengths of Band II are larger than d (below the light line). When d is smaller than the resonant wavelength of Band III, this mode can also be excited, as shown in Fig. 5(i). In contrast to only one single resonance observed in the shallow grooved waveguide at the same air gap of 555 μm [Fig. 5(c)], multiple resonances found in deep grooved waveguide signify a definitely different mechanism since the high order cavity modes in the groove can be greatly excited [Figs. 5(g)–5(i)]. Consequently, the decrease in air gap leads to a concentration of the energy into a deep groove area for a fundamental cavity mode. When the air gap is smaller than the resonant wavelength of high order cavity modes, such high order modes can be obtained and observed in transmission spectrum.

Finally, we make a simple comparison of our proposed structure with some similar structure as shown in [10,13] in THz region. Since the single groove structure inside the waveguide corresponds to the resonant features in the transmission spectra, our structure can operate as a multiband notch filter by using a single deep groove, which is very different from the single band notch filter based on one shallow grooved TE (TEM) mode PPWG [10,13]. Although the measured absorption rate is small in Fig. 3 compared with other work [8–10], some unique points of the current work can be obtained. First, besides the finding of new phenomenon (multiple resonances with single grooves), we verified that the origin of it contributes to a high order cavity mode in the deep groove; second, we found the novel phenomenon of resonant frequency deviation for a fundamental cavity mode (Band I) with a small air gap but different depth, which is because the THz field fully penetrates the deep groove. Moreover, by mechanically tuning the air gap, a multiband THz notch filter with the control of band number can be realized. It is worth noting that the depth h can also be deeper to excite higher order cavity modes and achieve the control of more bands.

In conclusion, a tunable multiband terahertz notch filter is presented experimentally and numerically based on a PPWG with a single deep groove. The adjustable air gap has been investigated to flexibly modify the filtering characteristics of the presented filter. There is no prominent shift in the transmission dip of fundamental cavity mode as the air gap is small and decreased. This air gap parameter can also be varied in the application to adjust the band number. The interesting fact in this phenomenon is the emergence of high order cavity modes in deep grooves. Because the air gap can be easily tunable by mechanical control or electrical adjustment, this deep grooved PPWG structure has great potential applications in THz spectroscopy and communication.

This work was partly supported by the National Program on Key Basic Research Project of China (973 Program, 2014CB339806); National Natural Science Foundation of China (11174207, 61138001, 61205094, 61307126); Major National Development Project of Scientific Instrument and Equipment (2011YQ150021, 2012YQ14000504), the Key Scientific and Technological Project of Shanghai Municipality (12142200100); Shanghai Rising-Star Program (14QA1403100); Program of Shanghai Subject Chief Scientist (14XD1403000); and Basic Research Key Project (12JC1407100).

References

1. R. Mendis and D. Grischkowsky, Opt. Lett. **26**, 846 (2001).
2. M. Nagel, P. H. Bolivar, and H. Kurz, Semicond. Sci. Technol. **20**, S281 (2005).
3. S. S. Harsha, N. Laman, and D. Grischkowsky, Appl. Phys. Lett. **94**, 091118 (2009).
4. J. Kitagawa, M. Kodama, S. Koya, Y. Nishifuji, D. Armand, and Y. Kadoya, Opt. Express **20**, 17271 (2012).
5. R. Mendis, V. Astley, J. Liu, and D. M. Mittleman, Appl. Phys. Lett. **95**, 171113 (2009).
6. E. S. Lee, J.-K. So, G.-S. Park, D. Kim, C.-S. Kee, and T.-I. Jeon, Opt. Express **20**, 6116 (2012).
7. E. S. Lee, S.-G. Lee, C.-S. Kee, and T.-I. Jeon, Opt. Express **19**, 14852 (2011).
8. L. Chen, C. M. Gao, J. M. Xu, X. F. Zang, B. Cao, and Y. M. Zhu, Opt. Lett. **38**, 1379 (2013).
9. V. Astley, K. S. Reichel, J. Jones, R. Mendis, and D. M. Mittleman, Appl. Phys. Lett. **100**, 231108 (2012).
10. E. S. Lee and T. Jeon, Opt. Express **20**, 29605 (2012).
11. R. Mendis and D. M. Mittleman, Opt. Express **17**, 14839 (2009).
12. R. Mendis and D. M. Mittleman, J. Opt. Soc. Am. B **26**, A6 (2009).
13. V. Astley, B. McCracken, R. Mendis, and D. M. Mittleman, Opt. Lett. **36**, 1452 (2011).
14. L. Chen, Z. Q. Cao, F. Ou, H. G. Li, Q. S. Shen, and H. C. Qiao, Opt. Lett. **32**, 1432 (2007).
15. X. S. Lin and X. G. Huang, Opt. Lett. **33**, 2874 (2008).
16. M. Yosuke, O. Toshihiro, H. Masanobu, F. Masuo, and N. Masatoshi, Opt. Express **16**, 16314 (2008).
17. X. Piao, S. Yu, S. Koo, K. Lee, and N. Park, Opt. Express **19**, 10907 (2011).
18. L. Chen, J. M. Xu, C. M. Gao, X. F. Zang, B. Cai, and Y. M. Zhu, Appl. Phys. Lett. **103**, 251105 (2013).
19. L. Chen, Y. M. Zhu, X. F. Zang, B. Cai, Z. Li, L. Xie, and S. L. Zhuang, Light Sci. Appl. **2**, e60 (2013).